JOURNAL OF MECHANICS OF CONTINUA AND MATHEMATICAL SCIENCES
www.journalimcms.org

ISSN (Online) : 2454 -7190 Vol.-20, No.-6, July (2025) pp 1 - 19 ISSN (Print) 0973-8975

NUMERICAL EXPLORATION OF CHEMICAL REACTION AND JOULE HEATING EFFECTS ON THE DYNAMICS OF THNF $Cu-TiO_2-SiO_2/H_2O$:HEAT AND MASS TRANSMISSION ANALYSIS

B. Naga Lakshmi[1], Ch. Maheswari[2], Venkata Rao Kanuri[3]
J. V. Ramanaiah[4], R. S. Durga Rao[5], V. S. Bhagavan[6]

[1]Department of Mathematics, Vignan Nirula Institute of Technology and Science for Women, Guntur - 522009, Andhra Pradesh, India.

[2]Department of Mathematics, Narasaraopeta Engineering College (Autonomous), Narasaraopet - 522601, Andhra Pradesh, India.

[3]Department of Engineering Mathematics, SRKR Engineering College Bhimavaram - 534204, Andhra Pradesh, India.

[4]Department of Humanities and Basic Sciences, Aditya University Surampalem, 533437, Andhra Pradesh, India.

[5]Department of Humanities and Basic Sciences, Vishnu Institute of Technology, Vishnupur, Bhimavaram -534202, Andhra Pradesh, India.

[6]Department of Engineering Mathematics, Koneru Lakshmaiah Education Foundation, Guntur-522302, Andhra Pradesh, India.

Email: evurimokshita@gmail.com,cmaheswari2014@gmail.com
k.ravi.msc@gmail.com, shyamsundar.medinty@medinty@acet.ac
venkataramanaiah.jammisetti@acet.ac.in, drvsb002@kluniversity.in

Corresponding Author: **B. Naga Lakshmi**

https://doi.org/10.26782/jmcms.2025.07.00001

(Received: April 12, 2025; Revised: June 23, 2025; Accepted: July 05, 2025)

Abstract

This analysis attempts to explain the theoretical analysis of Joule heating and chemical reactions on the systematic flow of a ternary hybrid nanofluid. The flow of the tri-nanofluids was examined on thermal, momentum, and concentration boundary layers (BL). The physical problem was developed as a partial differential equation (PDEs). This was changed to total differential equations by suitable similarity variables. The Runge-Kutta, along with the shooting technique, was employed on the transformed flow equations. These solutions were presented in a pictorial form to discuss the physical problem, while the quantities of interest in engineering are tabulated. The Eckert number was found to enhance the thermal analysis by elevating the temperature along with the velocity distribution. The Joule heating along the magnetic field in the analysis was discovered to limit the speed of the fluid by reducing the velocity distribution.

Keywords: Chemical reaction, Heat and Mass Transmission Analysis, Ternary hybrid nanofluid, Viscous dissipation.

I. Introduction

The study of chemically reacting nanofluids has recently been considered in the literature tremendously. Chemical reactions occur when new materials that are not the same as the reacting substances are produced. Ternary hybrid nanofluids, influenced by Joule heating and chemical reactions, play a vital role in different engineering and industrial applications. They are widely used in cooling systems for electronics and batteries, ensuring efficient heat dissipation and preventing overheating [II]. In chemical processing, these fluids enhance reaction rates and mass transport, optimizing production efficiency. Aerospace and automotive industries utilize them for effective thermal management in engines and spacecraft. Additionally, they have biomedical applications, such as cancer hyperthermia treatment and targeted drug delivery. Their role in renewable energy systems, including solar collectors and waste heat recovery, further highlights their importance in enhancing thermal performance and energy efficiency. In chemical engineering, they are employed in catalytic reactors to improve heat and mass transfer, leading to more efficient and controlled chemical synthesis [XIX]. Many authors in the literature have examined chemically reacting fluids due to their numerous applications. Al Turef et al. [IV] recently explained how it numerically simulates heat transport and mass transfer in ternary hybrid nanofluid flow over a wedge geometry, considering chemical reactions and activation energy. Nihaal et al. [XXI] explore the combined effect of Joule heating, viscous dissipation, and activation energy on THNF flow over various geometries, and K. Karthik et al. [XIV] discussed the effects of thermal radiation and thermophoretic particle displacement on THNF flow across a wedge. The unsteady flow of a ternary hybrid nanofluid between parallel plates, influenced by chemical reaction and activation energy, was analyzed by Bilal et al. [VII], and M. Arshad et al. [VI] investigated the flow of rotating hybrid nanofluids with thermal radiation and chemical reaction between parallel plates. Ramzan et al. [XXIII] explored chemically reacting THNF flows past a non-isothermal, along with non-isosolutal geometries. Sajid et al. [XXVI] examined traces of chemically reacting alongside Arrhenius energy in a ternary hybrid nanofluid through a wedge. Bilal et al. [VIII] studied chemically reacting MHD hybrid nanofluid flow past a plane by using thermal enhancement. Lakshmi et al. [XVIII] analysed chemical reaction impacts on incompressible laminar flow, three-dimensional, permeable, rotating hybrid nanofluid (Al_2O_3-Cu/H_2O) over a stretching sheet.

The examination of the ternary hybrid nanofluid (THN) has recently attracted many researchers in the literature. Many studies in the literature have examined it through heat analysis and observed its significance on heat enhancement. This new form of hybrid nanofluid finds applications in climate control, automobile water retention, turbine-conditioned behaviour, etc. Alqawasmi et al. [III] explored THN dynamics using a numerical approach with the Fourier heat flux model. Khan et al. [XV] explored ferro-copper/blood-based nanofluid dynamics by optimizing the entropy between two stretching disks. Farooq et al. [XI] determined an insight into manganese zinc ferrite nanoparticles by analyzing kerosene oil conveying silver. Khan

Muhammad Naveed et al. [XVI] analyze heat transfer of chemically reactive micropolar Williamson THNF flow with Joule heating and over diffusion effects. Alshahrani et al. [IV] elucidated the dynamics of a ternary nanofluid with thermal jump and multiple slip constraints. The study of Alqawasmi Khaled et al. [III] presents a numerical approach to the study flow and heat transfer of THNF upon spinning disk. The systematic flow of THN in a stretchable sheet symmetrically was elucidated by Priyadharshini et al. [XXII]. Raza et al. [XXIV] elucidated the tri-hybrid nanofluid based on the role of the nanolayer subject to nanoparticles morphology through two porous disks. Humera Khan Humera et al. [XVII] recently discussed the properties of Gyrotactic microorganisms present in a ternary hybrid nanofluid that flows between two spinning discs. Guedri et al. [XII] explained thermal behaviour on the dynamics of THN past a non-linear stretchable sheet.

The viscous dissipative role of the fluid dynamics within the boundary layer has attracted researchers recently. However, the heat transport analysis enhancement with viscous dissipation is a more interesting aspect due to its applications in industries are due to a very high thermal conductivity. Ethylene glycol, water, and oil have low thermal conductivity. Due to this, many studies have concentrated on the impact of viscous dissipation on the heat enhancement of many other nanofluids. Rehman Ali et al. [XXV] present a detailed analysis for viscous dissipation over the transient magnetohydrodynamic flow of Casson nanofluid above a stretchy surface, with a particular focus on optimizing thermal regulation in advanced engineering systems. Various studies explore the analytical solutions of Poiseuille flow in rotating inclined pipes, while some examine the analytical expressions for velocity, temperature, and Nusselt numbers in Couette-Poiseuille flow of power-law fluids, considering viscous dissipation by Coelho Paule et al., V R Kanuri et al. [X, XIII]. Boubaker et al. [IX] elucidated insight into viscous dissipative Power-law fluids by utilizing the discretization method. Ahmed et al. [I] explored the insight into Joule and viscous dissipation on magnetohydrodynamic boundary layer dynamics for viscoelastic fluid.

To the very most of our knowledge, there is no study in the literature, and it was considered a theoretical exploration of Joule heating and the chemical reaction effect on the dynamics of ternary hybrid nanofluid. Having this in mind, our focus in this paper is to explain the numerical approach to solve the equations of motion describing the physical problem under exploration, as well as explaining the impact of significant parameters on the flow. The numerical method is utilized by considering a guess with an accurate value by explaining the expression of the solution.

II. Mathematical formulation

Consider an incompressible, steady, and electrically conducting tri-composite nanoparticles water-based ternary hybrid nano-fluid flows through an inclined plane. We considered that the nanoparticles consist, Copper (Cu), Titanium oxide (TiO_2), and Silicon oxide (SiO_2) is explored with water as the base fluid. A magnetism of uniform strength (B_0) was imposed in a perpendicular direction to the inclined plane. The heat and mass transmission analysis was governed by control parameters such as joule heating, chemical reaction, thermal radiation, and heat generation, respectively.

The inclined plane surface explaining the flow phenomena is shown in **Figure 1**. The concentration and temperature of the flow of fluid situated at the free stream, as well as the wall, are C_w, T_w, C_∞ and T_∞ respectively. The levels of species concentration are considered to be very low, such that Soret and Dufour mechanisms are ignored.

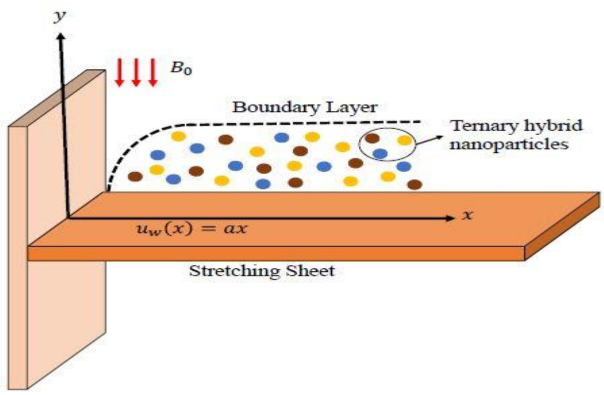

Fig. 1. Geometry for the flow problem

Based on the approximation for the boundary layer, the governing flow equations are [XXII]:

$$\frac{\partial u}{\partial x}+\frac{\partial v}{\partial y}=0 \tag{1}$$

$$\rho_{thnf}\left(u\frac{\partial u}{\partial x}+v\frac{\partial u}{\partial y}\right)=\mu_{thnf}\frac{\partial^2 u}{\partial y^2}-\sigma_{thnf}B_0^2u+\rho_{thnf}[g\beta_t(T-T_\infty)]\cos(\alpha)-\frac{\mu_{thnf}}{K_0}u \tag{2}$$

$$u\frac{\partial T}{\partial x}+v\frac{\partial T}{\partial y}=\frac{k_{thnf}}{(\rho c_p)_{thnf}}\frac{\partial^2 T}{\partial y^2}+\frac{Q_c}{(\rho c_p)_{thnf}}(T-T_\infty)-\frac{1}{(\rho C_p)_{thnf}}\frac{\partial q_r}{\partial y}+\frac{\mu_{thnf}}{(\rho C_p)_{thnf}}\left(\frac{\partial u}{\partial y}\right)^2 \tag{3}$$

$$u\frac{\partial C}{\partial x}+v\frac{\partial C}{\partial y}=D_B\frac{\partial^2 C}{\partial y^2}-K_1(C-C_\infty) \tag{4}$$

Corresponding Boundary constraints are:

$$\text{At } y=0, u=U_{w,} v=0, k_{thnf}\frac{\partial T}{\partial y}=-h_t(T_w-T), D_B\frac{\partial C}{\partial y}=-(C_w-C)$$

$$\text{As } y\to\infty,\ C\to C_\infty, T\to T_\infty, u\to 0. \tag{5}$$

The radiating heat fluxes were encountered during the fluid flow with the utilization of Rosseland diffusion approximation, such that:

$$q_r=-\frac{4\sigma_s}{3ke}\frac{\partial T^4}{\partial y} \tag{6}$$

By utilizing the Rosseland approximation, the heat and mass transmission analysis of the work examined optically thin liquids. By taking note of the difference in temperature to be so small that equation (7) is transformed to a linear form by evaluating T^4 using Taylor's techniques in T_∞ and avoiding the higher terms leads to:

$$T^4 \cong 4T_\infty^3 T - 3T_\infty^4 \tag{7}$$

The energy equation becomes:

$$u\frac{\partial T}{\partial x} + v\frac{\partial T}{\partial y} = \frac{k_{thnf}}{(\rho c_p)_{thnf}}\frac{\partial^2 T}{\partial y^2} + \frac{Q_c}{(\rho c_p)_{thnf}}(T - T_\infty) + \frac{16\sigma_s T_\infty^3}{3ke(\rho C_p)_{thnf}}\frac{\partial^2 T}{\partial y^2} + \frac{\mu_{thnf}}{(\rho C_p)_{thnf}}\left(\frac{\partial u}{\partial y}\right)^2 \tag{8}$$

To change the flow equation analysis into ODEs, the well-defined similarity variables are:

$$u = axf'(\eta), v = -(av)^{\frac{1}{2}} f(\eta), \theta(\eta) = \frac{T - T_\infty}{T_w - T_\infty}, \phi(\eta) = \frac{C - C_\infty}{C_w - C_\infty}, \eta = \left(\frac{a}{v}\right)^{\frac{1}{2}} y \tag{9}$$

Utilizing equation (9) above on the heat and mass transmission flow analysis to obtain:

$$A_1 f''' + A_2(ff'' - f'^2) + Gr\cos(\alpha)\theta - (A_3 M + A_1 K)f' = 0 \tag{10}$$

$$\left(A_4 + R\right)\theta'' + \Pr\Delta_f\theta + A_1 Ec\Pr f''^2 + A_5\Pr f\theta' = 0 \tag{11}$$

$$\phi'' + Scf\phi' - ScKr\phi = 0 \tag{12}$$

Where

$$A_1 = \frac{\mu_{thnf}}{\mu_f}, A_2 = \frac{\rho_{thnf}}{\rho_f}, A_3 = \frac{\sigma_{thnf}}{\sigma_f}, A_4 = \frac{k_{thnf}}{k_f}, A_5 = \frac{(\rho C_p)_{thnf}}{(\rho C_p)_f}.$$

along the constraints:

$$f(0) = 1, f'(0) = 0, \theta'(0) = -\frac{\gamma}{A_4}(1 - \theta(0)), \phi'(0) = -\beta(1 - \phi(0)),$$
$$f'(\infty) = 0, \theta(\infty) = 0, \phi(\infty) = 0. \tag{13}$$

$$M = \frac{\sigma_f B_0^2}{a\rho_f}, Gr = \frac{g\beta_t(T_w - T_\infty)}{a^2 x}, K = \frac{\nu_f}{aK_0}, R = \frac{16\sigma_s T_\infty^3}{3kek_f}, \Pr = \frac{\nu_f\left(\rho C_p\right)_f}{k_f},$$
$$Ec = \frac{(ax)^2}{(c_p)_f(T_w - T_\infty)}, \Delta_f = \frac{Q_c}{(\rho c_p)_f a}, Sc = \frac{\nu_f}{D_B}, Kr = \frac{K_1}{a} \tag{14}$$

The above are the magnetic parameter, thermal Grashof number, permeability, thermal radiation, heat generation, Eckert number, and Prandtl number, respectively. The quantities of engineering interest for momentum and thermal boundary layer are described as follows:

$$C_{fx}=\frac{(\mu)_{thnf}}{\mu_f a x^2}\left(\frac{\partial u}{\partial y}\right)_{y=0},\ Nu_x=-\left(\frac{\partial T}{\partial y}\right)_{y=0}\frac{x k_{thnf}}{k_f(T_w-T_\infty)}\ \text{ and }\ Sh_x=-x\left(\frac{\partial C}{\partial y}\right)_{y=0}$$

By implementing the similarity variables to obtain:

$$C_{fx}=\frac{\mu_{thnf}}{\mu_f}\frac{f''(0)}{\sqrt{\mathrm{Re}_x}}\ \text{ and }\ Nu_x=\frac{k_{thnf}}{k_f}\theta'(0)\sqrt{\mathrm{Re}_x},\quad \mathrm{Re}_x^{-1/2}Sh_x=-\phi'(0).$$

Table 1: Ternary Hybrid Nanofluids correlations [XXIV]

Properties	**Ternary Hybrid Nanofluid**
Viscosity	$\mu_{thnf}=\frac{\mu_f}{(1-\phi_1)^{2.5}(1-\phi_2)^{2.5}(1-\phi_3)^{2.5}}$
Density	$\rho_{thnf}=\left[(1-\phi_2)\left[(1-\phi_3)+\phi_3\frac{\rho_3}{\rho_f}\right]+\phi_2\frac{\rho_2}{\rho_f}\right](1-\phi_1)+\phi_1\frac{\rho_1}{\rho_f}$
Electrical conductivity	$\frac{\sigma_{thnf}}{\sigma_{hnf}}=\frac{(1-2\phi_1)\sigma_{hnf}+(1+2\phi_1)\sigma_1}{(1+\phi_1)\sigma_{hnf}+(1-\phi_1)\sigma_1}$, $\frac{\sigma_{hnf}}{\sigma_{nf}}=\frac{(1-2\phi_2)\sigma_{nf}+(1+2\phi_2)\sigma_2}{(1+\phi_2)\sigma_{nf}+(1-\phi_2)\sigma_2}$, $\frac{\sigma_{nf}}{\sigma_f}=\frac{(1+2\phi_3)\sigma_3+(1-2\phi_3)\sigma_f}{(1-\phi_3)\sigma_3+(1+\phi_3)\sigma_f}$
Thermal conductivity	$\frac{k_{nf}}{k_f}=\frac{k_3+2k_f-2\phi_3(k_f-k_3)}{k_3+2k_f-\phi_3(k_f-k_3)}$, $\frac{k_{hnf}}{k_{nf}}=\frac{k_2+2k_{nf}-2\phi_2(k_{nf}-k_2)}{k_2+2k_{nf}-\phi_2(k_{nf}-k_2)}$, $\frac{k_{thnf}}{k_{hnf}}=\frac{k_1+2k_{hnf}-2\phi_1(k_{hnf}-k_1)}{k_1+2k_{hnf}-\phi_1(k_{hnf}-k_1)}$
Heat capacity	$(\rho c_p)_{thnf}=\left[(1-\phi_2)\left[(1-\phi_3)+\phi_3\frac{(\rho c_p)_3}{(\rho c_p)_f}\right]+\phi_2\frac{(\rho c_p)_2}{(\rho c_p)_f}\right](1-\phi_1)+\phi_1\frac{(\rho c_p)_1}{(\rho c_p)_f}$

Table 2: Thermophysical properties of $Cu, TiO_2,\ SiO_2\ /\ H_2O$ [XXIV]

Properties	H_2O	TiO_2	Cu	SiO_2
$k(w/mk)$	0.6071	8.953	400	1.4013
$c_p(J/kgk)$	0.4179	686.2	385	765
$\rho(kg/m^3)$	0.997	4250	8933	2270
$\sigma(s/m)$	$(5.5)(10^{-6})$	$(2.4)(10^{6})$	1.67	$(3.5)(10^{6})$

III. Methodology

The systems of ODEs were tackled numerically using Runge-Kutta techniques alongside the shooting techniques. To implement the R-K techniques, the system was first changed into a system of first-order ODEs. The shooting technique was utilized on the total coupled equations.

$$f = y_1, \frac{df}{d\eta} = \frac{dy_1}{d\eta} = y_2, \frac{d^2 f}{d\eta^2} = \frac{d}{d\eta}\left(\frac{dy_1}{d\eta}\right) = \frac{dy_2}{d\eta} = y_3, \frac{d^3 f}{d\eta^3} = \frac{d}{d\eta}\left(\frac{dy_2}{d\eta}\right) = \frac{dy_3}{d\eta} \quad (15)$$

$$\theta = y_4, \frac{d\theta}{d\eta} = \frac{dy_4}{d\eta} = y_5, \quad \frac{d^2\theta}{d\eta^2} = \frac{d}{d\eta}\left(\frac{dy_4}{d\eta}\right) = \frac{dy_5}{d\eta} \quad (16)$$

$$\varphi = y_6, \frac{d\phi}{d\eta} = \frac{dy_6}{d\eta} = y_7, \frac{d^2\phi}{d\eta^2} = \frac{d}{d\eta}\left(\frac{dy_6}{d\eta}\right) = \frac{dy_7}{d\eta}. \quad (17)$$

Substituting equations (15), (16), and (17) into the transformed equations to obtain:

$$\left(A_4 + R\right)\frac{dy_5}{d\eta} + \Pr\Delta_f y_4 + A_1 Ec \Pr y_3^2 + A_5 \Pr y_1 y_5 = 0. \quad (18)$$

$$\frac{dy_7}{d\eta} + Scy_1 y_7 - ScKry_6 = 0. \quad (19)$$

along the constraints:

$$y_7(0) = -\beta(1 - y_6(0)), y_5(0) = -\frac{\gamma}{A_4}(1 - y_4(0)), y_2(0) = 0, y_1(0) = 1 \quad (20)$$

$$y_6(\infty) = 0, y_4(\infty) = 0, y_2(\infty) = 0. \quad (21)$$

Simplifying equations (16) and (17) to obtain:

$$\frac{dy_3}{d\eta} = \frac{(A_3 M + A_1 K)y_2 + A_2\left(y_2^2 - y_1 y_3 - Gr\cos(\alpha)y_4\right)}{A_1} \quad (22)$$

$$\frac{dy_5}{d\eta} = \frac{-\left(\Pr\Delta_f y_4 + A_1 Ec \Pr y_3^2 + A_5 \Pr y_1 y_5\right)}{\left(A_4 + R\right)}. \quad (21)$$

$$\frac{dy_7}{d\eta} = ScKry_6 - Scy_1 y_7. \quad (22)$$

IV. Results and discussion

This paper conducted a numerical insight into $Cu + TiO_2 + SiO_2/\ H_2O$ THN with Joule heating, additionally, viscous dissipative effects. The physical problem represented by PDEs and changed to ODEs was tackled by utilizing the Runge-Kutta method along with the shooting approach. Pictorial graphs were used to analyze the impact of pertinent flow parameters on the solute concentration, velocity, and temperature. In addition, the qualities of engineering interest are tabulated.

Figure 2 illustrates that the thermal Grashof number (Gr) affects, within the range $1.5 \leq Gr \leq 3.0$, on the velocity profile. Here, Gr shows a perceptible rise in the fluid velocity profile. Because Gr represents a buoyancy-driven force that promotes the upward motion of the fluid. The reason for this is that increasing the Grashof number causes a decrease in the viscosity of the nanofluid, which aids flow acceleration and momentum diffusion. As a result, the velocity distribution is enhanced as the Grashof number increases. Furthermore, the thermal Grashof number and buoyancy forces are precisely proportional.

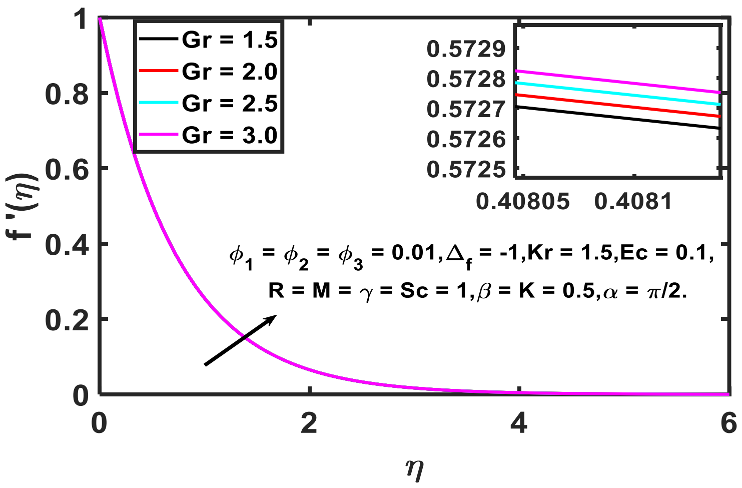

Fig. 2. velocity distribution of K

Figures 3-5 exemplify the influence of the porosity (K), within the range $1 \leq K \leq 4$, which represents the increase of porosity within the fluid, on velocity, temperature, and concentration profiles of the Cu-TiO_2-SiO_2/H_2O (THN) flow. Porosity refers to the presence of voids or pores within a material, and an upsurge in the permeability parameter corresponds to a higher porosity level. As K increases, the temperature and concentration profiles reveal an ascending trend, while the velocity profile shows a declining behaviour. This inverse relationship is credited to the enhanced viscous forces associated with higher porosity, which suppress the fluid motion by increasing flow resistance and allowing inertial forces to dominate. Accordingly, heat transfer from the heated surface to the fluid intensifies, resulting the elevated flow temperatures. Also, increased porosity generates a resistive force opposing the flow, which contributes to the enhancement of concentration distribution within the boundary layer. **Figure 6** demonstrates the inclination angle (α) impact within the range $0 \leq \alpha \leq \frac{\pi}{2}$, on the velocity profile of the Cu-TiO_2-SiO_2/H_2O THN fluid flow. It is observed that increasing α significantly results in a decline in the velocity profile. This behaviour is credited to a reduction in buoyancy forces as the inclination angle grows, causing a decrease in fluid velocity.

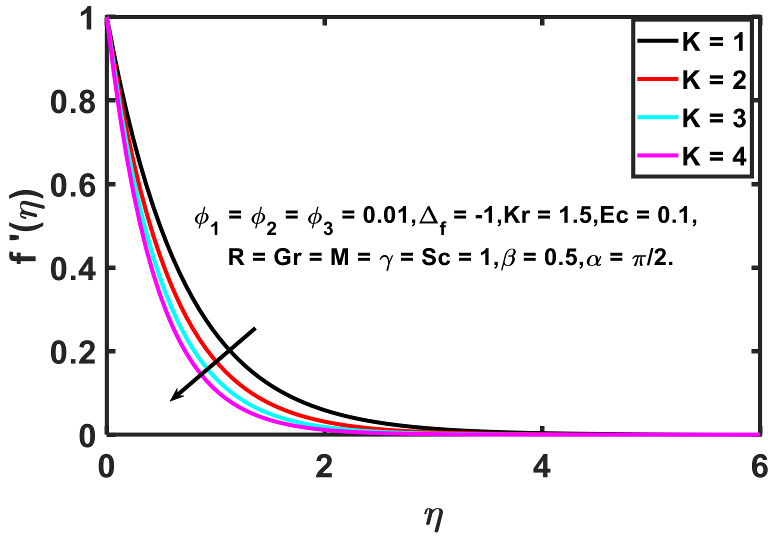

Fig. 3. velocity distribution of K

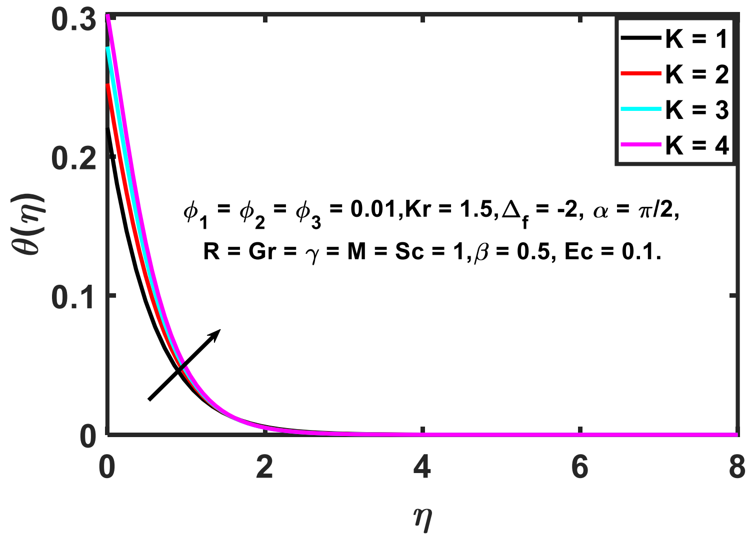

Fig. 4. temperature distribution of K

Figure 7 highlights the effect of magnetic parameter (M), within the range $2 \leq M \leq 5$, on velocity distribution. An increase in M leads to a perceptible drop in velocity. Applied magnetic field engenders a Lorentz force, which resists the mobility of the flow and consequently slows down the flow, thereby thinning the momentum boundary layer. **Figure 8** exemplifies the temperature of the fluid with the effect of the heat generation/sink parameter (Δ_f). When Δ_f value increases in a hybrid nanofluid flow, the temperature profile also increases.

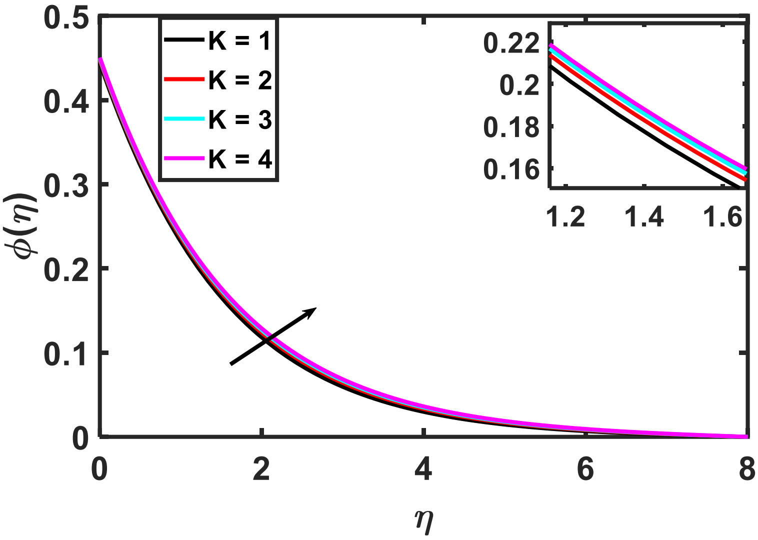

Fig. 5. concentration distribution of K

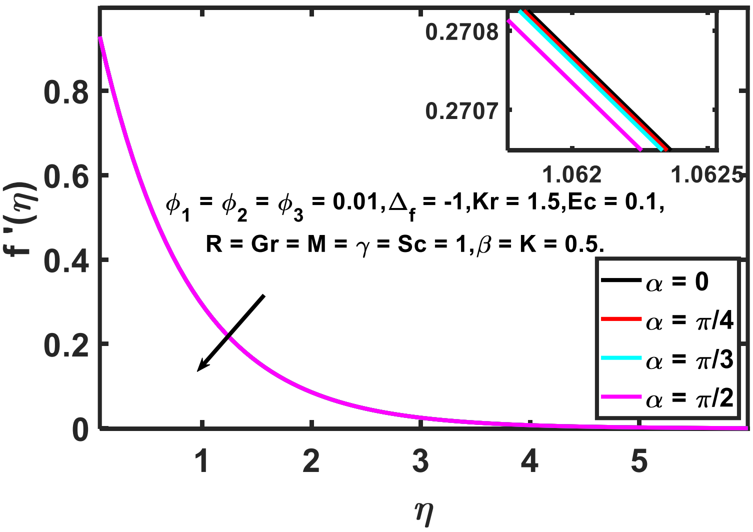

Fig. 6. velocity distribution of α

Figure 9 depicts the influence of Eckert number, within the span $0.1 \leq Ec \leq 0.4$, on the temperature profiles. The Eckert number suggests the influence of enthalpy and kinetic energy within the flow system. It signifies the conversion of kinetic energy into internal energy as a result of work against viscous forces in the fluid. As the dissipative heat increases, it causes a corresponding temperature rise.

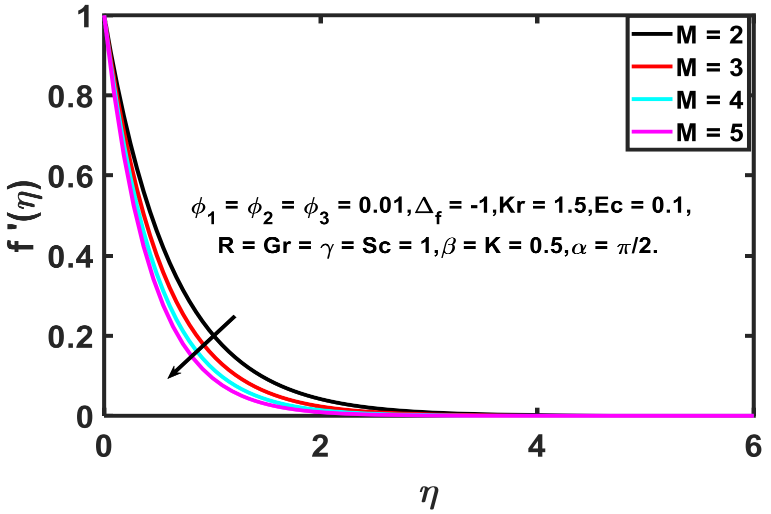

Fig. 7. velocity distribution of M

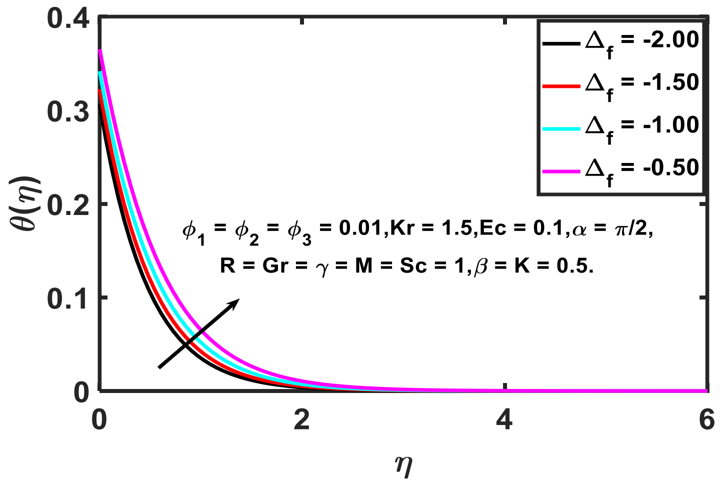

Fig. 8. temperature distribution of Δ_f

Figure 10 elucidates the influence of thermal radiation (R), within the range $1 \leq R \leq 4$, on the temperature distribution. It is pragmatic that the temperature profile rises when an upsurge in R. The cause is that when R is enhanced, the additional quantity of energy is deposited in the ternary hybrid nanoliquid particles and the compounded thickness of the momentum boundary layer. As a result, increasing R improves the temperature distribution. The current study reveals that the absorption of thermal radiation within the fluid layer affects both the thermal boundary layer thickness and the temperature. Subsequently, the interaction of thermal and radiative effects becomes more prominent within the boundary layer.

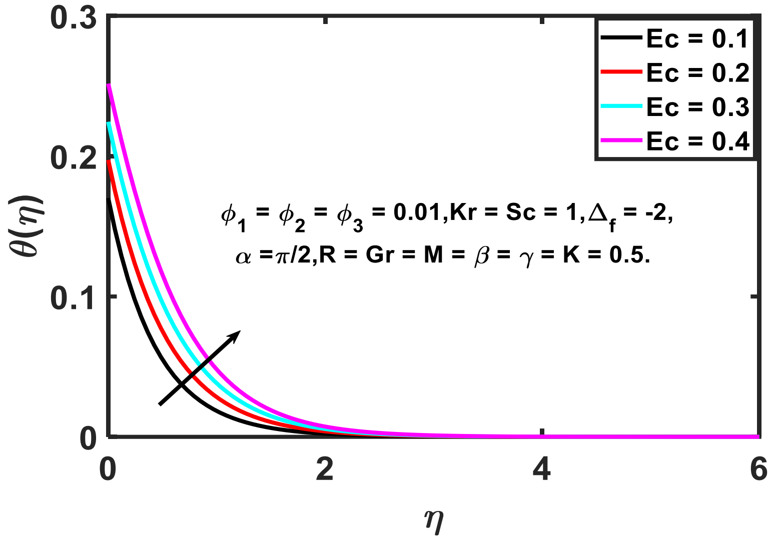

Fig. 9. temperature distribution of Ec

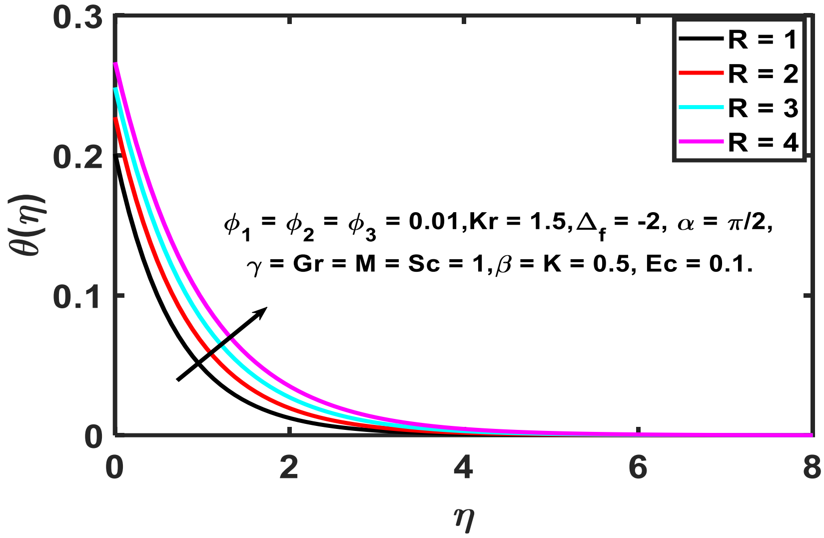

Fig. 10. temperature distribution of R

Figures 11 and 12 depict the impact of thermal slip $(1 \leq \gamma \leq 4)$ and concentration slip $(1 \leq \beta \leq 4)$ on temperature and concentration profiles of THN fluid flow, respectively. A rise in thermal slip enhances the temperature profile, indicating a greater effect on heat transfer. Similarly, concentration slip notably affects the concentration distribution, where increasing values of β result in a higher concentration profile.

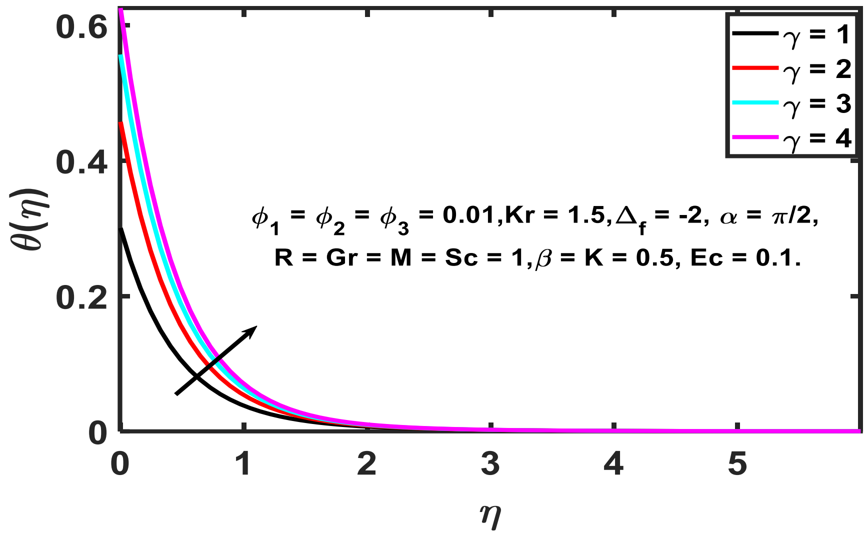

Fig. 11. temperature distribution of γ

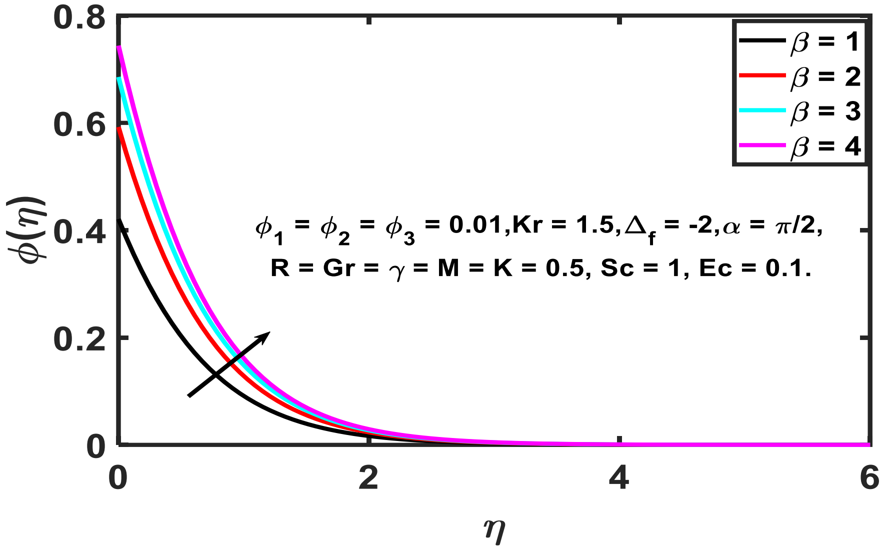

Fig. 12. concentration distribution of β

Figure 13 presents the Schmidt number effect, within the range $1 \leq Sc \leq 1.75$, on the concentration profile. The results show that an increase in Sc causes a decrease in concentration. This behavior is attributed to the fact that higher *Sc* values correspond to lower mass diffusivity, resulting in a reduced concentration distribution within the fluid. **Figure 14** demonstrates the impact of chemical reaction (Kr), within the range $1.00 \leq Kr \leq 1.75$, on the THN fluid flow. It is observed that the concentration profile declines with an increase in Kr. This behavior has been explained by the fact that a stronger chemical reaction enhances the consumption of nanomaterials, resulting in a decreased concentration as Kr increases.

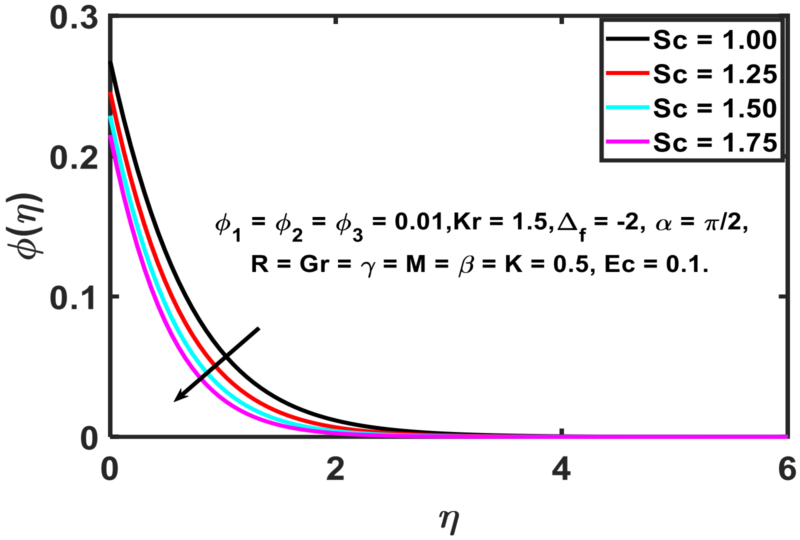

Fig. 13: concentration distribution of Sc

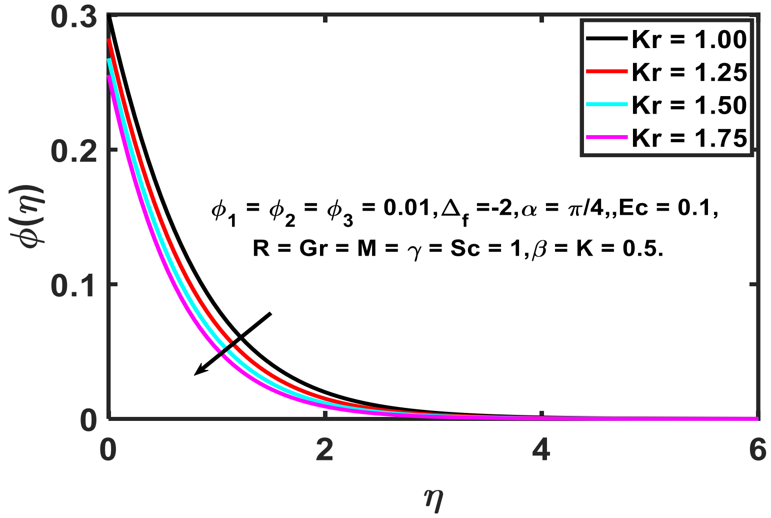

Fig. 14: concentration distribution of Kr

Table 3 presents data demonstrating the effects of various non-dimensional parameters, namely Gr, α, M, Ec, R, *Δf*, Sc, Kr, γ, and β on key physical quantities. It is noticed that an intensification in both the magnetic parameter (M) and the thermal diffusivity leads to a notable reduction in the skin friction coefficient, while the other parameters appear to have negligible influence on it. Likewise, Nusselt number increases with higher values of the radiation parameter (R), but exhibits a declining trend with rising M, α, Ec, γ, and *Δf*. Changes in the remaining parameters do not significantly affect the Nusselt number. As for the Sherwood number, it generally increases with greater values of M, whereas it tends to decrease when Sc, Kr, and β are elevated. No considerable variation in the Sherwood number is examined with changes in the other parameters.

Table 3: Skin friction coefficient ($C_f \mathrm{Re}_x^{\frac{1}{2}}$), Nusselt number ($Nu_x \mathrm{Re}_x^{-\frac{1}{2}}$), and Sherwood number ($Sh_x \mathrm{Re}_x^{-\frac{1}{2}}$) impact on Cu-$TiO_2$-$SiO_2$/$H_2O$ ternary hybrid nanofluids.

Gr	***α***	***M***	***Ec***	***R***	***Δf***	***Sc***	***Kr***	***γ***	***β***	$\sqrt{Re}\,C_{fx}$	$Re^{-\frac{1}{2}}\,Nu_x$	$Re^{-\frac{1}{2}}\,Sh_x$
0.1										-1.08270	2.720219	-0.310130
0.2										-1.08270	2.720219	-0.310130
0.3										-1.08270	2.720219	-0.310130
0.4										-1.08270	2.720219	-0.310130
	0									-1.08249	2.720430	-0.310132
	π/6									-1.08252	2.720401	-0.310132
	π/2									-1.08255	2.720368	-0.310132
	π/3									-1.08260	2.720324	-0.310131
		0.1								-0.83711	2.674723	-0.367493
		0.2								-0.90475	2.553992	-0.367279
		0.3								-0.96770	2.456956	-0.367084
		0.4								-1.02681	2.377263	-0.366907
			3							-1.08270	1.632741	-0.350859
			4							-1.08270	1.271969	-0.350859
			5							-1.08270	1.041778	-0.350859
			6							-1.08270	0.882135	-0.350859
				0.01						-1.08270	1.898736	-0.310130
				0.02						-1.08270	1.915903	-0.310130
				0.03						-1.08270	1.933051	-0.310130
				0.04						-1.08270	1.950180	-0.310130
					-0.10					-1.08270	2.720219	-0.310130
					-0.11					-1.08270	2.804016	-0.310130
					-0.12					-1.08270	2.884500	-0.310130
					-0.13					-1.08270	2.962042	-0.310130
						0.1				-1.08270	2.720219	-0.137542
						0.2				-1.08270	2.720219	-0.148782
						0.3				-1.08270	2.720219	-0.158925
						0.4				-1.08270	2.720219	-0.168136
							0.1			-1.08270	9.200250	-0.286184
							0.2			-1.08270	9.200250	-0.286184
							0.3			-1.08270	9.200250	-0.286184
							0.4			-1.08270	9.200250	-0.286184
								4.0		-1.08270	2.674723	-0.350859
								4.5		-1.08270	2.553992	-0.350859
								5.0		-1.08270	2.456956	-0.350859
								5.5		-1.08270	2.377263	-0.350859
									0.1	-1.08270	2.720219	-0.089091
									0.2	-1.08270	2.720219	-0.160657
									0.3	-1.08270	2.720219	-0.219405
									0.4	-1.08270	2.720219	-0.268496

Table 4 gives comparison results for $\theta'(0)$ for various values of Pr when $\phi_1 = \phi_2 = \phi_3 = R = 0$. The investigation shows that there is excellent agreement between the current computations and the literature that has been published.

Table 4 : Comparison results for $\theta'(0)$, various values of *Pr*

Pr	Manjunatha et al. [XX]	Priyadarshini et al. [XXII]	Present work
2.0	0.9113	0.9114	0.9113
7.0	1.8954	1.8954	1.8953
20	3.3539	3.3539	3.3538

V. Conclusion

In this study, the theoretical analysis of Joule heating and chemical reaction impact on dynamics of $(Cu + TiO_2 + SiO_2 / H_2O)$ is explored. The outcomes of pertinent flow parameters are obtained on concentration, temperature, and velocity graphs. The equation governing the fluid motion is solved numerically with a convergence rate of 10^{-6}. The key conclusions are as follows:

- An increase in the thermal Grashof number (Gr) enhances fluid velocity and leads to a thicker boundary layer.
- Higher inclination angle (α) contributes to a reduction in the fluid velocity. Elevating the magnetic parameter (M) results in a clear decline in velocity due to the magnetic damping effect.
- As the porosity parameter (K) rises, temperature and concentration profiles both are
  increase, while the velocity profile decreases.
- In this ternary hybrid nanofluid flow, a greater heat generation/sink parameter (Δ_f) corresponds to an increase in the temperature distribution. Eckert number (Ec), which accounts for the conversion of internal energy from kinetic energy, influences thermal behaviour within the system. Radiation parameter (R) leads to a higher temperature profile, indicating enhanced heat transfer due to radiative effects.
- Thermal slip conditions are found to elevate the temperature distribution in the flow field. Similarly, concentration slip acts as a key role in modifying solutal transport, where higher values of the slip parameter (β) amplify the concentration profile.
- A rise in Sc results in reduced concentration, signifying lower mass diffusivity. An intensification of chemical reaction (Kr) leads to a decline in the concentration profile due to stronger reactive effects.

VI. Applications

This research provides useful insights that may be applied in a variety of sophisticated technology domains. In terms of thermal management, it promotes increased cooling efficiency for electronics and automotive systems that operate in electrically affected situations. The outcomes can also help optimise coolant behaviour in energy sources like nuclear reactors and solar thermal systems. In the biomedical area, regulated heat generation and chemical reactivity help to further targeted treatments such as hyperthermia and precision medication delivery. Slip effects allow us to model realistic flows at micro and nano scales, enhance heat and mass transfer predictions, adjust boundary layer thickness, increase flow characteristics, and decrease energy losses.

Conflict of Interest:

There is no conflict of interest regarding this paper.

References

I. Ahmed, Saleem, Huma Iram, and Asif Mahmood. *"Joule and Viscous Dissipation Effects on MHD Boundary Layer Flow over a Stretching Sheet with Variable Thickness." International Journal of Emerging Multidisciplinaries in Mathematics*, vol. 1, no. 2, 2022, pp. 1–10. 10.54938/ijemdm.2022.01.2.27

II. Al Garalleh, Hakim. *"Numerical Simulation of Heat Transport Mechanism in Chemically Influenced Ternary Hybrid Nanofluid Flow over a Wedge Geometry." Discover Applied Sciences*, vol. 6, no. 9, 2024, p. 449. 10.1007/s42452-024-06141-4

III. Alqawasmi, Khaled, et al. *"Numerical Approach toward Ternary Hybrid Nanofluid Flow with Nonlinear Heat Source-Sink and Fourier Heat Flux Model Passing through a Disk." International Journal of Thermofluids*, vol. 18, 2023, p. 100367. 10.1016/j.ijft.2023.100367

IV. Alshahrani, Saad, et al. *"Numerical Simulation of Ternary Nanofluid Flow with Multiple Slip and Thermal Jump Conditions." Frontiers in Energy Research*, vol. 10, 2022, p. 967307. 10.3389/fenrg.2022.967307

V. Al-Turef, Gadah Abdulrahman, et al. *"Computational Study and Application of the Hamilton and Crosser Model for Ternary Hybrid Nanofluid Flow Past a Riga Wedge with Heterogeneous Catalytic Reaction." Nano*, vol. 20, no. 1, 2025, p. 2450105. 10.1142/S1793292024501054

VI. Arshad, Mubashar, et al. *"Rotating Hybrid Nanofluid Flow with Chemical Reaction and Thermal Radiation between Parallel Plates." Nanomaterials*, vol. 12, no. 23, 2022, p. 4177. 10.3390/nano12234177

VII. Bilal, Muhammad, et al. *"Numerical Analysis of an Unsteady, Electroviscous, Ternary Hybrid Nanofluid Flow with Chemical Reaction and Activation Energy across Parallel Plates." Micromachines*, vol. 13, no. 6, 2022, p. 874. 10.3390/mi13060874

VIII. Bilal, Muhammad, et al. *"Numerical Simulations through PCM for the Dynamics of Thermal Enhancement in Ternary MHD Hybrid Nanofluid Flow over Plane Sheet, Cone, and Wedge." Symmetry*, vol. 14, no. 11, 2022, p. 2419. 10.3390/sym14112419

IX. Boubaker, Karem, et al. *"Effects of Viscous Dissipation on the Thermal Boundary Layer of Pseudoplastic Power-Law Non-Newtonian Fluids Using Discretization Method and the Boubaker Polynomials Expansion Scheme." International Scholarly Research Notices*, vol. 2012, no. 1, 2012, p. 181286. 10.5402/2012/181286

X. Coelho, Paulo M., and Robert J. Poole. *"Heat Transfer of Power-Law Fluids in Plane Couette–Poiseuille Flows with Viscous Dissipation." Heat Transfer Engineering*, vol. 41, no. 13, 2020, pp. 1189–1207. 10.1080/01457632.2019.1611139

XI. Farooq, Umar, et al. *"Analysis of Kerosene Oil Conveying Silver and Manganese Zinc Ferrite Nanoparticles with Hybrid Nanofluid: Effects of Increasing the Lorentz Force, Suction, and Volume Fraction." Ain Shams Engineering Journal*, vol. 15, no. 1, 2024, p. 102326. 10.1016/j.asej.2023.102326

XII. Guedri, Kamel, et al. *"Thermal Flow for Radiative Ternary Hybrid Nanofluid over Nonlinear Stretching Sheet Subject to Darcy–Forchheimer Phenomenon." Mathematical Problems in Engineering*, vol. 2022, no. 1, 2022, p. 3429439. 10.1155/2022/3429439

XIII. Kanuri, Venkat Rao, et al. *"Investigating Poiseuille Flows in Rotating Inclined Pipes: An Analytical Approach." International Journal of Heat and Technology*, vol. 42, no. 1, 2024, pp. 329–336. 10.18280/ijht.420135

XIV. Karthik, K., et al. *"Impacts of Thermophoretic Deposition and Thermal Radiation on Heat and Mass Transfer Analysis of Ternary Nanofluid Flow across a Wedge." International Journal of Modelling and Simulation*, 2024, pp. 1–13. 10.1080/02286203.2023.2298234

XV. Khan, Humera, et al. *"Insights into the Significance of Ternary Hybrid Nanofluid Flow between Two Rotating Disks in the Presence of Gyrotactic Microorganisms." Nano*, 2024, p. 2450110. 10.1142/s1793292024501108

XVI. Khan, Muhammad Naveed, et al. *"Flow and Heat Transfer Insights into a Chemically Reactive Micropolar Williamson Ternary Hybrid Nanofluid with Cross-Diffusion Theory." Nanotechnology Reviews*, vol. 13, no. 1, 2024, p. 20240081. 10.1515/ntrev-2024-0081

XVII. Khan, Shan Ali, et al. *"Entropy Optimized Ferro-Copper/Blood Based Nanofluid Flow between Double Stretchable Disks: Application to Brain Dynamic." Alexandria Engineering Journal*, vol. 79, 2023, pp. 296–307. 10.1016/j.aej.2023.08.017

XVIII. Lakshmi, Bhavanam Naga, et al. *"Numerical Analysis of Three-Dimensional Magneto Hybridized Nanofluid (Al_2O_3-Cu/H_2O) Radiative Stretchable Rotating Flow with Suction." Engineering, Technology & Applied Science Research*, vol. 14, no. 5, 2024, pp. 16902–16910. 10.48084/etasr.8183

XIX. Li, Shuguang, et al. *"Aspects of an Induced Magnetic Field Utilization for Heat and Mass Transfer Ferromagnetic Hybrid Nanofluid Flow Driven by Pollutant Concentration." Case Studies in Thermal Engineering*, vol. 53, 2024, p. 103892. 10.1016/j.csite.2023.103892

XX. Manjunatha, S., et al. *"Theoretical Study of Convective Heat Transfer in Ternary Nanofluid Flowing Past a Stretching Sheet." Journal of Applied and Computational Mechanics*, vol. 8, no. 4, 2022, pp. 1279–1286. 10.22055/jacm.2021.37698.3067

XXI. Nihaal, Kandavkovi Mallikarjuna, et al. *"Combined Impact of Joule Heating, Activation Energy, and Viscous Dissipation on Ternary Nanofluid Flow over Three Different Geometries." International Journal of Computational Methods and Experimental Measurements*, vol. 11, no. 4, 2023, pp. 251–258. 10.18280/ijcmem.110407

XXII. Priyadharshini, P., et al. *"Ternary Hybrid Nanofluid Flow Emerging on a Symmetrically Stretching Sheet Optimization with Machine Learning Prediction Scheme." Symmetry*, vol. 15, no. 6, 2023, p. 1225. 10.3390/sym15061225

XXIII. Ramzan, Muhammad, et al. *"A Theoretical Analysis of the Ternary Hybrid Nanofluid Flows over a Non-Isothermal and Non-Isosolutal Multiple Geometries." Heliyon*, vol. 9, no. 4, 2023. 10.1016/j.heliyon.2023.e14875

XXIV. Raza, Qadeer, et al. *"Numerically Analyzed of Ternary Hybrid Nanofluids Flow of Heat and Mass Transfer Subject to Various Shapes and Size Factors in Two-Dimensional Rotating Porous Channel." Case Studies in Thermal Engineering*, vol. 56, 2024, p. 104235. 10.1016/j.csite.2024.104235

XXV. Rehman, Ali, et al. *"Viscous Dissipation Effects on Time-Dependent MHD Casson Nanofluid over Stretching Surface: A Hybrid Nanofluid Study." Journal of Molecular Liquids*, vol. 408, 2024, p. 125370. 10.1016/j.molliq.2024.125370

XXVI. Sajid, Tanveer, et al. *"Trace of Chemical Reactions Accompanied with Arrhenius Energy on Ternary Hybridity Nanofluid Past a Wedge." Symmetry*, vol. 14, no. 9, 2022, p. 1850. 10.3390/sym14091850